ACS OMEGA

http://pubs.acs.org/journal/acsodf

Article

BODIPY Dimers with a Fused and Coplanar Structure: Photophysical Comparison, Low Threshold for Amplified Spontaneous Emission, and Deep-Red Bio-Imaging/Photodynamic Therapy Application

Yang Wang,* Qinning Sun, Lei Xie, Long Chen, Fengrong Zhu, and Liang Liu

Cite This: *ACS Omega* 2023, 8, 28376−28386

Read Online

ACCESS | Metrics & More | Article Recommendations | Supporting Information

ABSTRACT: Boron dipyrromethene (BODIPY)-derived dyes are generally superior emitters, but their absorption and emission fail to match the bio-active optical window (650−900 nm). In this work, we explored four bisBODIPY dyes (PB1−PB4) with easy-to-go synthesis, good solubility, high photostability, and high emission quantum yield in the deep-red region. Methyl and ethyl groups were introduced in these BODIPY dyes to improve their solubility. PB4 having a fused coplanar plane was synthesized and compared to PB1−PB3 having a non-fused structure. Their geometric structure was confirmed by single-crystal analysis, and their electronic structure, along with one-photon and two-photon absorptions, was analyzed by time-dependent functional theory calculation. Their absorption/emission spectra, emission quantum yields, and lifetimes were compared. It was found that the fused coplanar structure successfully red shifted PB4 absorption/emission to the deep-red region (698/720 nm), with a quantum yield of 0.58. PB4 showed an amplified spontaneous emission effect with an output efficiency of 6.0% at a pumping power of 3000 μJ. An improved photodynamic therapy (PDT) performance was observed from PB4 via in vitro and in vivo experiments. The practical PDT performance was evaluated by cell availability. Upon a 980 nm laser radiation of 5 min, the cell viability was decreased to ∼15%.

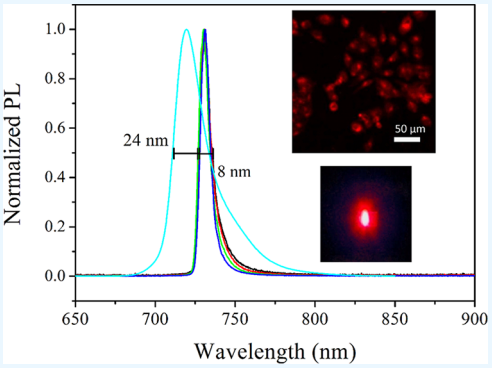

1. INTRODUCTION

The development for optoelectronic devices, lighting, and imaging techniques requires superior photosensitizers, dyes, and emitters to meet various demands in practical applications.[1−3] Among the numerous candidates based on inorganic phosphors, quantum dots, carbon dots, polymers, and metal complexes, pure organic dyes are always attractive due to their virtues of the versatile structure, tunable band gap, flexibility, and good solubility. Especially, owing to their wide applications in noninvasive and in vivo bio-imaging, organic dyes working within the near-infrared region (NIR, 650−900 nm) have attracted much research attention.[4] Boron dipyrromethene (BODIPY)-derived dyes have shown superior emissive performance, including high emission quantum yield, high molar extinction coefficient, and stable structure, which endows them with various applications in bio-imaging, organic lasing, amplified spontaneous emission (ASE), and even photodynamic therapy (PDT).[5−7] The classic BODIPY skeleton has intense absorption and efficient emission at ∼500 nm, which mismatches the transparent window for bio-applications (650−900 nm).[7] To solve this problem, various chemical modifications on the BODIPY skeleton have been tried, hoping to shift the absorption/emission to the NIR/deep-red optical window (650−900 nm), such as grafting linear or cyclic aromatic moieties, replacing the *meso*-C with the N atom, and constructing conjugated oligomers.[8−13] Nevertheless, with the successfully decreased energy gap between HOMO (highest occupied molecular orbital) and LUMO (lowest unoccupied molecular orbital), emissive performance is weakened as well, showing a decreased emission quantum yield. This is because the introduced substituents (groups) have intense structural relaxation in the excited state, which exhausts emissive energy. Some new neat design on the BODIPY skeleton thus should be performed, aiming at a high emission quantum yield in the NIR/deep-red optical window.

Recently, by adopting a conjugated and fused structure, several BODIPY dyes having a high emission quantum yield in the NIR optical window have been successfully reported. For example, as reported by Kolemen and coworkers, a bisBODIPY structure was designed via an α,α-benzene fused ring.[13] Similarly, another bisBODIPY structure was reported by Bennniston and coworkers following a β,β-benzene fused

Received: April 13, 2023
Accepted: July 17, 2023
Published: July 26, 2023

Scheme 1. Synthetic Route for PB1−PB4

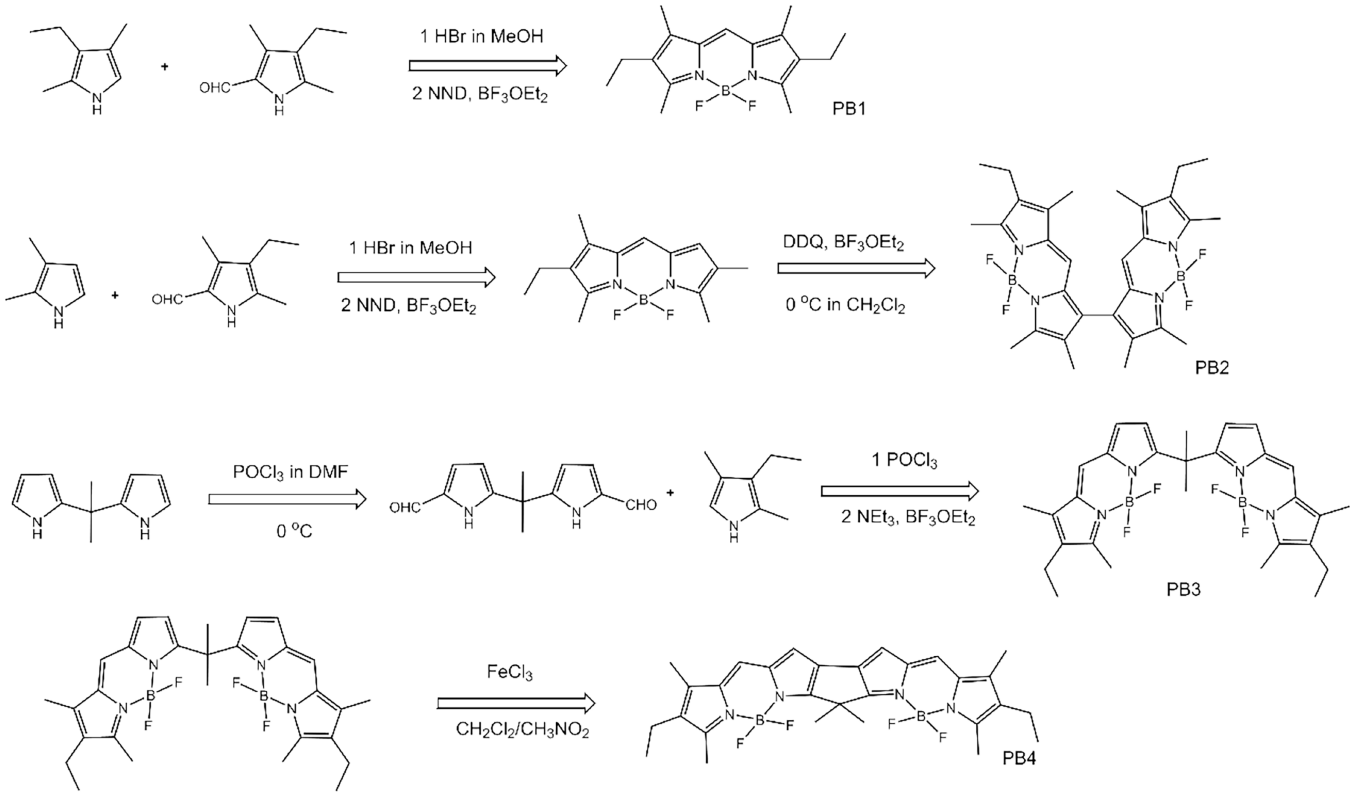

ring.[14] Additionally, Li and coworkers reported a BODIPY trimer with a pyrazine fused structure through an oxidation of the β-amino precursor.[15] Regardless of their intense absorption/emission bands in the NIR optical window, these bisBODIPY dyes necessitated laborious and comprehensive synthesis, which made their further application limited and unwelcome. Another disadvantage that comes with the benzene-fused-ring bisBODIPY structure is the compromised solubility in common solvents, which prevents these bisBODIPY structures from applications in the field of bio-imaging and organic lasing.

Guided by the above consideration, we intend to explore bisBODIPY dyes with easy-to-go synthesis, good solubility, high photostability, and high emission quantum yield in the NIR/deep-red optical window. As shown in Scheme 1, in this work, three bisBODIPY dyes (PB2, PB3, and PB4) were designed, along with a reference monoBODIPY dye (PB1). Methyl and ethyl groups were introduced in these BODIPY dyes, hoping to improve their solubility. PB2 and PB3 had a non-fused structure, while PB4 had a coplanar fused structure. A full comparison between these dyes was performed, and their potential application in bio-imaging and PDT was explored as well.

2. EXPERIMENTAL SECTION

2.1. General Information. A general synthetic procedure for PB1−PB4 is shown in Scheme 1. The starting reagents were commercially purchased and used as received without further notice, including 2′,7′-dichlorofluorescin diacetate (DCFH-DA), 3-ethyl-2,4-dimethyl-1*H*-pyrrole, 2,3-dimethyl-1*H*-pyrrole, 4-ethyl-3,5-dimethyl-1*H*-pyrrole-2-carbaldehyde, 2,2′-(propane-2,2-diyl)bis(1*H*-pyrrole), trifluoroacetic acid (TFA), 2,3-dichloro-5,6-dicyano-1,4-benzoquinone (DDQ), *N*,*N*-diisopropylethylamine (NND), 1,3-diphenylisobenzofuran (DPBF), $BF_3{\cdot}Et_2O$, $HBr{\cdot}H_2O$ (48%), $POCl_3$, $FeCl_3$, and NEt_3. Organic solvents, such as CH_2Cl_2 and *N*,*N*-dimethylformamide (DMF), were purified before usage with standard procedures. Compounds were characterized on a Bruker Avance 300 spectrometer (NMR), an Agilent 1100 MS spectrometer (MS), and a Bruker SMART APEX II X-ray single-crystal diffractometer (single-crystal XRD). The absorption and emission spectra were determined using a Hitachi F-7000 fluorescence spectrophotometer and a Shimadzu UV-3101PC spectrophotometer. Laser power and spectra were recorded using an Ocean Optics Maya2000 Pro Fiber Optic spectrometer (excitation = Nd:YAG laser, 10 Hz, 10 ns) and Newport 2936C laser power meters.

2.2. Synthesis of PB1−PB4. 2,8-Diethyl-5,5-difluoro-1,3,7,9-tetramethyl-5*H*-4l4,5l4-dipyrrolo[1,2-*c*:2′,1′-*f*][1,3,2]-diazaborinine (PB1) was synthesized following a literature method, with a minor modification.[14] To a solution of 3-ethyl-2,4-dimethyl-1*H*-pyrrole (8.7 mmol) and 4-ethyl-3,5-dimethyl-1*H*-pyrrole-2-carbaldehyde (8.2 mmol) in MeOH (100 mL), HBr (48% in H_2O) was dropwise added and stirred at room temperature for 1 h. After the reaction, a mixed solvent of Et_2O/*n*-pentane (120 mL, v:v = 1:1) was added, and the resulting mixture was stirred for 24 h under an ice bath. The resulting red solid (dipyrrin hydrobromide) was collected and dried and then used directly for the next step. Yield: 78%.

The as-synthesized dipyrrin hydrobromide (2,8-diethyl-1,3,7,9-tetramethyldipyrrin hydrobromide, 6.5 mmol) was dissolved in CH_2Cl_2 (300 mL), and then NND (45 mmol) was added and stirred at room temperature for 10 min. Under an ice bath, $BF_3{\cdot}Et_2O$ (77 mmol) was dropwise added and stirred for another 1 h at room temperature. The resulting solution was washed with saturated Na_2CO_3 solution, and the

https://doi.org/10.1021/acsomega.3c02452
ACS Omega 2023, 8, 28376−28386

organic phase was vaporized to give a red solid, which was further purified on a silica gel column using *n*-pentane/CH_2Cl_2 (2:1) as the eluent. Yield: 91%. ^{1}H NMR (DMSO-d_6, 300 MHz) δ: 7.05 (s, 1H), 2.53−2.47 (m, 4H), 2.32−2.25 (m, 6H), 2.08 (d, J = 6.0 Hz, 6H), 1.12 (dd, J = 8.0 Hz, 6H). ^{13}C NMR (DMSO-d_6, 75 MHz) δ: 150.2, 147.5, 144.9, 142.9, 141.9, 130.4, 129.2, 128.1, 113.2, 20.4, 17.8, 17.3, 16.0, 15.1, 14.1, 11.9, 9.7. ^{11}B NMR (DMSO-d_6, 128 MHz) δ: −0.153 (t, J = 31.4 Hz). ^{19}F NMR (DMSO-d_6, 376 MHz) δ: −145.55 (q, J = 33.1 Hz). MS calculated for $C_{17}H_{23}BF_2N_2$: 304.2; found: m/z 304.2 [m]$^+$. Analytical calculation for $C_{17}H_{23}BF_2N_2$: C, 67.12; H, 7.62; N, 9.21. Found: C, 67.05; H, 7.80; N, 9.16. Its single crystal was obtained and discussed below.

8,8′-Diethyl-5,5,5′,5′-tetrafluoro-2,2′,3,3′,7,7′,9,9′-octamethyl-5*H*,5′*H*-4l4,5l4,5′l4,6′l4-1,1′-bidipyrrolo[1,2-*c*:2′,1′-*f*]-[1,3,2]diazaborinine (PB2) was synthesized by a two-step procedure. First, 2-ethyl-5,5-difluoro-1,3,7,8-tetramethyl-5*H*-4l4,5l4-dipyrrolo[1,2-*c*:2′,1′-*f*][1,3,2]diazaborinine was synthesized following the synthetic procedure for PB1, except that 3-ethyl-2,4-dimethyl-1*H*-pyrrole was replaced by 2,3-dimethyl-1*H*-pyrrole in this run. Yield: 70%. ^{1}H NMR (DMSO-d_6, 300 MHz) δ: 7.42 (s, 1H), 6.50 (s, 1H), 2.52−2.47 (m, 5H), 2.31 (s, 3H), 2.19 (s, 3H), 2.11 (s, 3H), 1.09 (t, J = 7.8 Hz, 3H).

The as-synthesized 2-ethyl-5,5-difluoro-1,3,7,8-tetramethyl-5*H*-4l4,5l4-dipyrrolo[1,2-*c*:2′,1′-*f*][1,3,2]diazaborinine (0.29 mmol) was dissolved in CH_2Cl_2 (60 mL), and then under an ice bath, $BF_3{\cdot}Et_2O$ (1.47 mmol) and DDQ (0.29 mmol) were slowly added. The mixture was stirred at 0 °C for 2 h and then washed with saturated Na_2CO_3 solution, and the organic phase was vaporized to give a purple-red solid, which was further purified on a silica gel column using *n*-pentane/CH_2Cl_2 (2:1) as the eluent. Yield: 64%. ^{1}H NMR (DMSO-d_6, 300 MHz) δ: 9.61 (s, 1H), 7.75 (s, 1H), 2.53−2.49 (m, 4H), 2.34−2.25 (m, 12H), 2.12−2.06 (m, 12H), 1.12−1.09 (dd, J = 8.0 Hz, 6H). ^{13}C NMR (DMSO-d_6, 75 MHz) δ: 150.9, 150.1, 147.0, 145.4, 144.9, 143.5, 141.9, 139.3, 132.8, 130.4, 129.4, 128.8, 128.0, 127.8, 117.4, 113.9, 113.5, 20.4, 17.8, 17.3, 16.2, 15.1, 14.1, 13.7, 12.0, 11.1, 9.7. ^{11}B NMR (DMSO-d_6, 128 MHz) δ: 1.19 (t, J = 33.0 Hz). ^{19}F NMR (DMSO-d_6, 376 MHz) δ: −146.6 (dq, J = 110 Hz, 34 Hz), −147.0 (dq, J = 110 Hz, 34 Hz). MS calculated for $C_{30}H_{36}B_2F_4N_4$: 550.3; found: m/z 550.3 [m]$^+$. Analytical calculation for $C_{30}H_{36}B_2F_4N_4$: C, 65.48; H, 6.59; N, 10.18. Found: C, 65.40; H, 6.67; N, 10.14. Its single crystal was obtained and discussed below.

2-Ethyl-7-(2-(8-ethyl-5,5-difluoro-7,9-dimethyl-5*H*-4l4,5l4-dipyrrolo[1,2-*c*:2′,1′-*f*][1,3,2]diazaborinin-3-yl)propan-2-yl)-5,5-difluoro-1,3-dimethyl-5*H*-4l4,5l4-dipyrrolo[1,2-*c*:2′,1′-*f*]-[1,3,2]diazaborinine (PB3) was synthesized following a two-step procedure. First, 5,5′-(propane-2,2-diyl)bis(1*H*-pyrrole-2-carbaldehyde) was synthesized following a literature method.[15] Under an ice bath, $POCl_3$ (12 mmol) was dropwise added into DMF (12 mmol) and stirred for 60 min. Then, CH_2Cl_2 (20 mL) was added. A solution of 2,2′-(propane-2,2-diyl)bis(1*H*-pyrrole) (5 mmol) in CH_2Cl_2 (50 mL) was dropwise added, and the resulting mixture was stirred at room temperature for 5 h. The reaction mixture was mixed with saturated Na_2CO_3 solution slowly and stirred for another 5 h. The organic phase was vaporized to give a pale yellow solid, which was further purified on a silica gel column using *n*-pentane/ethyl acetate (10:1) as the eluent. Yield: 59%. ^{1}H NMR (DMSO-d_6, 300 MHz) δ: 9.95 (s, 2H), 9.48 (s, 2H), 6.57 (d, J = 4.8 Hz, 2H), 6.12 (d, J = 4.8 Hz, 2H), 1.61 (s, 6H).

The as-synthesized 5,5′-(propane-2,2-diyl)bis(1*H*-pyrrole-2-carbaldehyde) was dissolved in toluene (1 mmol in 10 mL) and then mixed with 3-ethyl-2,4-dimethyl-1*H*-pyrrole solution in CH_2Cl_2 (2.5 mmol in 1 mL). Under an ice bath, $POCl_3$ solution in CH_2Cl_2 (1 mmol in 1 mL) was slowly added under an argon atmosphere. The resulting mixture was stirred at room temperature for 30 min, and then Et_3N (2 mL) was added and stirred for another 20 min; finally, $BF_3{\cdot}Et_2O$ (4 mL) was poured into this reaction mixture and stirred at 40 °C for 30 min. After the reaction, 100 mL of water and 30 mL of ethyl acetate were added. The organic phase was vaporized to give a red solid, which was further purified on a silica gel column using *n*-pentane/CH_2Cl_2 (2:1) as the eluent. Yield: 42%. ^{1}H NMR (DMSO-d_6, 300 MHz) δ: 7.43 (s, 1H), 7.13 (s, 1H), 7.02 (d, J = 3.6 Hz, 1H), 6.52−6.49 (d, J = 9.0 Hz, 2H), 6.17 (d, J = 2.4 Hz, 1H), 2.53−2.49 (m, 4H), 2.31−2.21 (m, 6H), 2.08−2.06 (d, J = 6.0 Hz, 6H), 1.61 (s, 6H), 1.12−1.08 (dd, J = 8.0 Hz, 6H). ^{13}C NMR (DMSO-d_6, 75 MHz) δ: 150.2, 149.3, 147.4, 145.1, 144.8, 143.8, 142.0, 128.4, 126.5, 122.3, 120.0, 114.7, 113.7, 112.1, 109.8, 45.7, 27.9, 20.4, 17.8, 17.3, 16.0, 15.1, 14.1, 11.9, 9.9. ^{11}B NMR (DMSO-d_6, 128 MHz) δ: −0.343 (t, J = 33.0 Hz). ^{19}F NMR (DMSO-d_6, 376 MHz) δ: −145.75 (dq, J = 102 Hz, 30.7 Hz), −144.97 (dq, J = 102 Hz, 32.2 Hz). MS calculated for $C_{29}H_{34}B_2F_4N_4$: 536.2; found: m/z 536.3 [m]$^+$. Analytical calculation for $C_{29}H_{34}B_2F_4N_4$: C, 64.96; H, 6.39; N, 10.45. Found: C, 64.91; H, 6.45; N, 10.36. Its single crystal was obtained and discussed below.

(*Z*)-5-((4-Ethyl-3,5-dimethyl-1*H*-pyrrol-2-yl)methylene)-2-((*Z*)-(4-ethyl-3,5-dimethyl-2*H*-pyrrol-2-ylidene)methyl)-7,7-dimethyl-5,7-dihydro-1*H*-cyclopenta[1,2-*b*:4,3-*b*′]dipyrrolo-[1,2-*c*:2′,1′-*f*][1,3,2]diazaborinine (PB4) was synthesized using PB3 as a starting compound. $FeCl_3$ solution in CH_3NO_2 (1 mmol in 5 mL) was dropwise added into PB4 solution in CH_2Cl_2 (0.1 mmol in 50 mL). After being stirred at room temperature for 5 min, saturated Na_2CO_3 solution (50 mL) and CH_2Cl_2 (30 mL) were added. The organic phase was vaporized to give a red solid, which was further purified on a silica gel column using *n*-pentane/CH_2Cl_2 (2:1) as the eluent. Yield: 72%. ^{1}H NMR (DMSO-d_6, 300 MHz) δ: 7.64 (s, 1H), 7.53 (s, 1H), 7.46 (s, 1H), 6.20 (s, 1H), 2.52−2.49 (m, 4H), 2.31−2.21 (m, 6H), 2.08−2.06 (d, J = 6.0 Hz, 6H), 1.45 (s, 6H), 1.12−1.09 (dd, J = 9.0 Hz, 6H). ^{13}C NMR (DMSO-d_6, 75 MHz) δ: 154.4, 151.4, 150.2, 147.8, 147.1, 146.7, 144.8, 142.0, 134.3, 128.4, 127.9, 126.4, 121.5, 120.3, 118.7, 115.2, 48.8, 26.6, 20.4, 17.8, 17.3, 16.0, 15.0, 14.1, 11.9, 9.8. ^{11}B NMR (DMSO-d_6, 128 MHz) δ: −0.103 (t, J = 33.0 Hz). ^{19}F NMR (DMSO-d_6, 376 MHz) δ: −146.08 (dq, J = 109 Hz, 32.3 Hz), −145.35 (dq, J = 109 Hz, 33.8 Hz). MS calculated for $C_{29}H_{32}B_2F_4N_4$: 534.2; found: m/z 534.3 [m]$^+$. Analytical calculation for $C_{29}H_{32}B_2F_4N_4$: C, 65.20; H, 6.04; N, 10.49. Found: C, 65.12; H, 6.13; N, 10.42. Its single crystal was obtained and discussed below.

2.3. ASE and Emission Quantum Yield Measurement.

For ASE performance evaluation, BODIPY solutions were prepared, and each solution was loaded in a quartz cell. A Q-switched Nd:YAG laser (1 Hz, 10 ns, 355 nm) was applied as the excitation source. The excitation beam was first modulated by a diaphragm and then divided into two sub-beams by a splitter (1:1). Sub-beam 1 was measured by a laser power meter (Newport 2936C) and sub-beam 2 (6 mm × 0.6 mm stripe) was focused onto the quartz cell through a cylindrical lens. The pumping laser direction was perpendicular to the

https://doi.org/10.1021/acsomega.3c02452
ACS Omega 2023, 8, 28376−28386

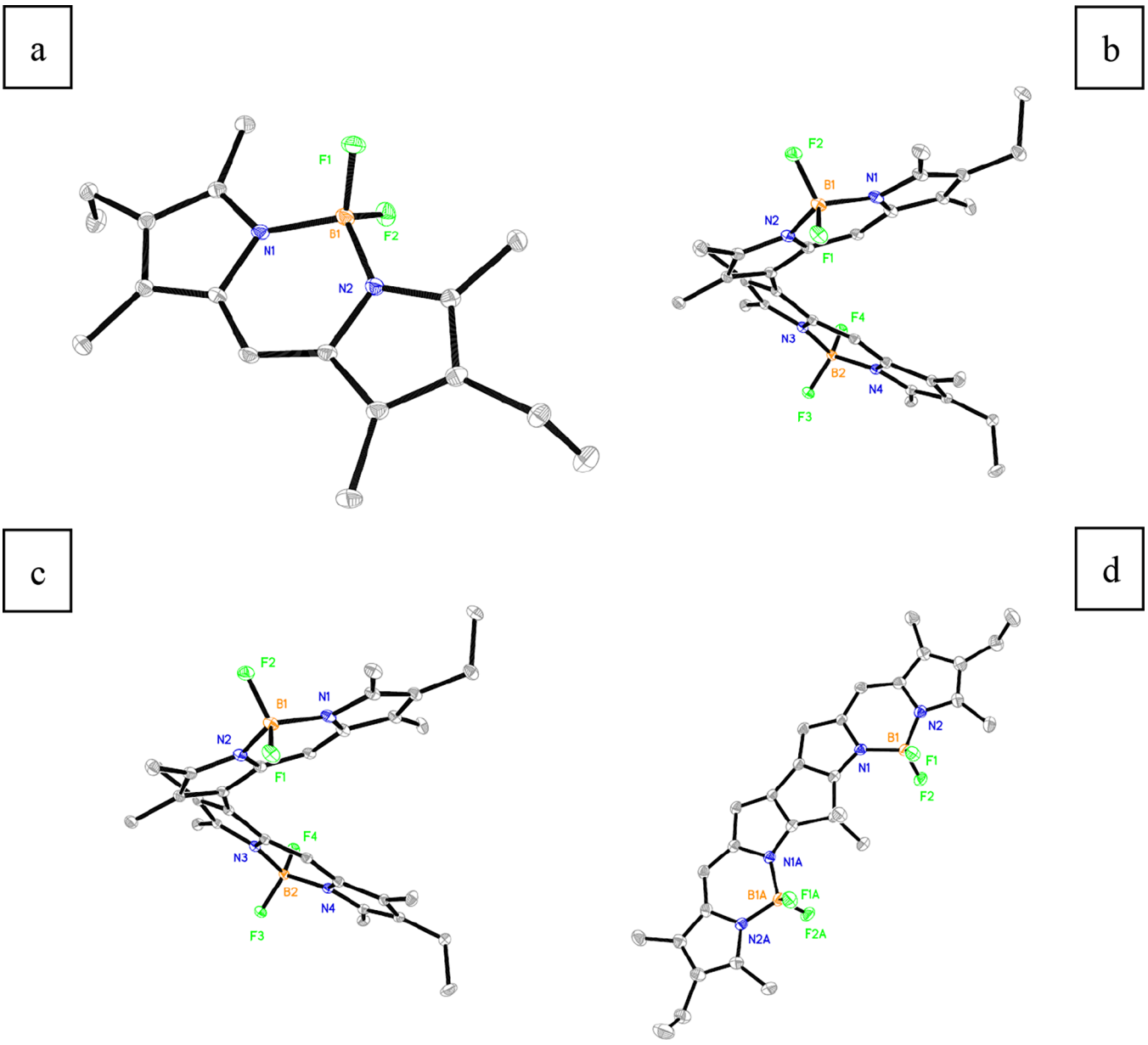

Figure 1. Single-crystal structures of PB1 (a), PB2 (b), PB3 (c), and PB4 (d). Detailed geometric parameters can be found from the Supporting Information.

focused sub-beam 2. The BODIPY ASE output power was calculated against the pumping power of sub-beam 1.

For steady fluorescence emission quantum yield (Φ) determination, a reference method was applied.[16] In Formula 1, Φ_X means BODIPY Φ, and Φ_{ST} is the Φ of a standard reference. $Grad_X$ and $Grad_{ST}$ are the integrated area values of the emission spectra from BODIPY and standard reference, and n_X and n_{ST} denote the refractive indices of the solvent, respectively. Here, fluorescein was dissolved in NaOH aqueous solution (0.1 M) and used as a reference (Φ_{ST} = 0.95).

$$\Phi_X = \Phi_{ST}\left(\frac{Grad_X}{Grad_{ST}}\right)\left(\frac{n_X^2}{n_{ST}^2}\right) \quad (1)$$

2.4. TD-DFT Analysis on PB1−PB4. Theoretical analysis on PB1−PB4 was performed by time-dependent density functional theory (TD-DFT) calculation in vacuum at the RB3LYP/6-31G(d) level.[17] Their single crystals were used as the initial geometry. One-photon absorption (OPA) and two-photon absorption (TPA) details were calculated by GAMESS-US in vacuum at the RB3LYP/6-31G(d) level. No solvent model was applied. Frontier molecular orbitals were plotted by wxMacMolPlt with a contour value of 0.03.

2.5. Photodynamic Performance Determination of PB1−PB4. For photodynamic performance determination, DPBF was chosen as an indicator for the generation of singlet O_2 ($^1O_2$). DPBF stock solution in ethanol (1 mM) was prepared in the dark room. Then, 2 mL of DPBF solution was mixed with the BODIPY dye (0.5 mM) in a quartz cell. After being treated with an ultrasonic bath for 3 min, this solution was exposed to 500 nm (for PB1−PB3) or 680 nm (for PB4) or continuous 980 nm radiation (0.1 W/cm^2, for PB1−PB4) generated by a 980 nm laser diode (CW NIR 980, 5 mW, Hi-Tech Optoelectronics Co., China). Its absorption spectrum and absorbance at 415 nm were recorded every 2 min.

https://doi.org/10.1021/acsomega.3c02452
ACS Omega 2023, 8, 28376−28386

2.6. Cell Cytotoxicity Assay and Bio-Imaging Performance of PB1−PB4. The cell cytotoxicity of PB4 was analyzed by MTT assays using HeLa cells, and here, MTT meant 3-(4,5-dimethylthiazol-2-yl)-2,5-diphenyltetrazolium bromide. Initially, HeLa cells (1×10^5) were cultured for 24 h, and then the BODIPY dye was added (2.0, 5.0, 10.0, 20.0, and 30.0 μM) and further cultured for 24 h. Then, a 980 nm laser (0.6 W/cm^2) was applied for 5 min or not (as a control). Finally, MTT solution (20 μL) was added and incubated at 37 °C for 4 h. By removing the medium, dimethyl sulfoxide (100 μL) was flushed, and the sample absorbance value was measured by a microplate reader (BioTek).

For bio-imaging performance evaluation, HeLa cells were incubated with the BODIPY dye (10.0 μM) at 37 °C for 1 or 5 h and then flushed by Dulbecco's phosphate-buffered saline (D-PBS, ×3). Cell imaging photos were recorded using an Olympus spectral confocal multiphoton microscope (FV1200-MPE, excitation = 635 nm). For the DCFH-DA/PB4 co-stain experiment, a similar operation was applied, but this time, DCFH-DA containing D-PBS was used. The excitation wavelength was set as 488 nm during DCFH-DA imaging. The power density of the 980 nm laser was 0.6 W/cm^2.

3. RESULTS AND DISCUSSION

3.1. BODIPY Synthesis Confirmed by NMR, MS, and Single-Crystal XRD. The successful synthesis of four BODIPY dyes (PB1−PB4) has been confirmed above in Section 2.2 by their characterization data, including NMR, MS, and elemental analysis. As mentioned above, PB1 has a basic BODIPY skeleton and is used as a reference compound. Meanwhile, PB2−PB4 are bisBODIPY dyes, and their methyl and ethyl groups are introduced so that the solubility of these bisBODIPY dyes shall not be compromised by their large conjugated planes. Especially, PB4 has a fused coplanar structure, which shall decrease the emissive energy to a deep-red optical window by narrowing the energy gap between HOMO and LUMO. On the other hand, PB4 shall still have a high emission quantum yield by controlling the energy-exhausting structural relaxation in the excited state. As a consequence, PB4 is supposed to be a good deep-red probe in bio-imaging and PDT.

The above hypothesis is first confirmed by their single-crystal structures shown in Figure 1 (see the Supporting Information for their detailed geometric parameters). As for PB1, a classic BODIPY structure is observed, while PB2 and PB3 have a twisted configuration with a dihedral angle of ∼73° owing to the steric hindrance between the two BODIPY skeletons. Such a large dihedral angle makes the conjugation between the two BODIPY skeletons ineffective. As expected, PB4 has a fused coplanar structure, which makes the conjugation between the two BODIPY skeletons rather effective. In addition, this fused structure is not flexible, so that the energy-exhausting structural relaxation in the excited state can be depressed. Thus, efficient NIR absorption/emission is expected from PB4.

3.2. Electronic Structure, OPA, and TPA Revealed by TD-DFT. The electronic structure of PB1−PB4, along with their OPA and TPA, is revealed by a time-dependent density functional theory (TD-DFT) method. A graphical presentation for their HOMO and LUMO is shown in Figure 2. As for PB1, its HOMO and LUMO are mainly localized on the BODIPY skeleton. As for PB2 and PB3, their twisted configuration makes the conjugation between its two BODIPY skeleton components inefficient; thus, the electronic distribution on one BODIPY skeleton is isolated from the other, showing poor conjugation. As for PB4, its coplanar plane structure makes the conjugation between its two BODIPY skeletons rather efficient, and the electronic distribution covers the whole molecular ring. Such a large size of conjugation shall effectively decrease the energy gap between HOMO and LUMO, shifting the transition energy from ∼500 nm for monoBODIPY to a deep-red optical window for a fused bisBODIPY structure.[7] And this statement is first confirmed by the calculated OPA energy values of PB1−PB4 as follows.

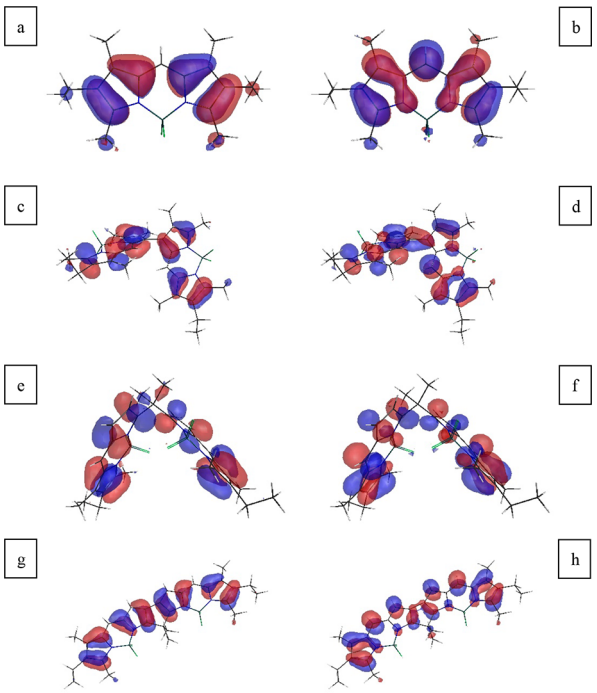

Figure 2. Graphic presentation for PB1 (a, HOMO; b, LUMO), PB2 (c, HOMO; d, LUMO), PB3 (e, HOMO; f, LUMO), and PB4 (g, HOMO; h, LUMO). The detailed TD-DFT calculation result can be found from the Supporting Information.

The singlet electronic excitation, which corresponds to OPA, is composed of a transition from HOMO to LUMO. The energy values of the first singlet electronic transition ($S_0 \rightarrow S_1$) are calculated as 2.956 eV for PB1, 2.363 eV for PB2, 2.520 eV for PB3, and 2.153 eV for PB4, respectively. With the increasing conjugation size, the $S_0 \rightarrow S_1$ transition energy is obviously decreased. A similar trend is observed for the other singlet electronic transitions ($S_0 \rightarrow S_n$, n = 2, 3, 4, and 5; see the Supporting Information for a detailed result of $S_0 \rightarrow S_n$, n = 1−5). This result actually means a spectral red shift for PB2−PB4, compared to PB1, which will be confirmed later by their absorption spectra. In addition, it is found that the $S_0 \rightarrow S_1$ oscillator strength of PB4 (1.0204) having a fused coplanar structure is much higher than that of PB1 (0.4705) having a basic BODIPY skeleton. This trend is observed for TPA oscillator strength as well, as shown in Table 1. The $TPA_{1,2}$ oscillator strength of PB4 (0.6771) is nearly 100-fold higher than that of PB1 (0.0098). Correspondingly, the polarization ratio of PB4 (1.5000) is higher than that of PB1 (1.4717). These increased factors of PB4 shall improve its optical performance, which will be discussed and confirmed later.

3.3. Photophysical Performance: Absorption, Emission, Quantum Yield, and Lifetime. As mentioned above,

https://doi.org/10.1021/acsomega.3c02452
ACS Omega 2023, 8, 28376−28386

Table 1. OPA ($S_0 \rightarrow S_n$) and TPA ($TPA_{m,n}$) Values Calculated by TD-DFT at the B3LYP/6-31G(d) Level in Vacuum[a]

	PB1		PB2		PB3		PB4	
transition	energy (eV)	oscillator strength	energy (eV)	oscillator strength	energy (eV)	oscillator strength	energy (eV)	oscillator strength
$S_0 \rightarrow S_1$	2.956	0.4705	2.363	0.1069	2.520	0.0557	2.153	1.0204
$S_0 \rightarrow S_2$	3.438	0.2508	2.391	0.0596	2.546	0.0005	2.452	0.0004
$S_0 \rightarrow S_3$	3.587	0.0553	2.825	0.3206	2.966	0.4888	3.080	0.0694
$S_0 \rightarrow S_4$	5.059	0.0363	3.004	0.2647	3.118	0.4247	3.151	0.2265
$S_0 \rightarrow S_5$	5.256	0.0006	3.016	0.1808	3.576	0.1003	3.400	0.2380
$TPA_{1,2}$	0.482	0.0098	0.028	0.0085	0.026	0.0629	0.299	0.6771
$TPA_{1,3}$	0.631	0.1021	0.462	0.0308	0.446	0.0000	0.926	0.1342
$TPA_{1,4}$	2.103	0.6297	0.641	0.0235	0.598	0.0004	0.998	0.0001
$TPA_{1,5}$	2.300	0.0020	0.653	0.0061	1.056	0.0010	1.247	0.0056
$TPA_{2,3}$	0.150	0.0337	0.434	0.0753	0.420	0.0672	0.627	0.0004
$TPA_{2,4}$	1.621	0.0359	0.613	0.0044	0.572	0.0000	0.699	1.1218
$TPA_{2,5}$	1.818	0.0021	0.625	0.0127	1.030	0.0016	0.947	0.0303
$TPA_{3,4}$	1.472	0.0143	0.179	0.0112	0.152	0.0014	0.071	0.0364
$TPA_{3,5}$	1.668	0.0003	0.191	0.0084	0.610	0.0051	0.320	0.0863
$TPA_{4,5}$	0.197	0.0001	0.012	0.0005	0.458	0.0117	0.249	0.0011

[a] m and n denote the state. See the Supporting Information for a detailed result.

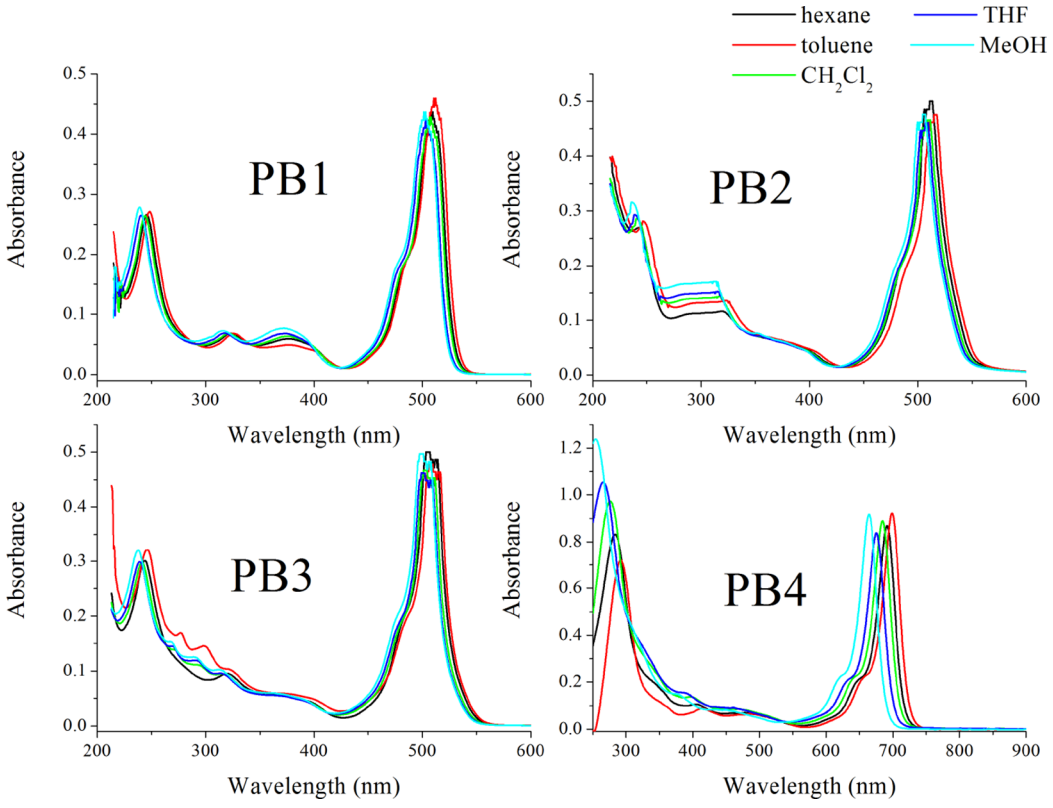

Figure 3. Absorption spectra of PB1−PB4 in various solvents (1 μM).

Table 2. Photophysical Parameters of PB1−PB4

	PB1	PB2	PB3	PB4
λ_{abs} (nm)[a]	509/511/507/504/502	511/514/512/507/504	509/511/507/505/503	692/698/685/676/663
λ_{em} (nm)[a,b]	526/530/523/527/528	532/539/537,613/534,616/536,616	533/528/528,611/526,613/529,634	716/720/712/713/718
Φ	0.61/0.77/0.62/0.48/0.36	0.41/0.43/0.27/0.35/0.31	0.44/0.40/0.35/0.33/0.30	0.46/0.58/0.51/0.52/0.39
τ (ns)[c]	13.1	5.7	2.9	7.1
ASE (μJ)[d]	1031	N/A	N/A	812

[a] Values were recorded in various solvents in sequence of hexane, toluene, CH_2Cl_2, THF, and MeOH; each value was separated with "/". [b] Values like "537,613" mean two emission peaks. [c] Measured in toluene, single exponential decay, for PB2 and PB3, the major emission band was selected. [d] ASE threshold energy determined as ASE output power equals to 20 μJ, measured in toluene (10 mM); N/A means no ASE effect even at a pumping powder of 3000 μJ.

https://doi.org/10.1021/acsomega.3c02452
ACS Omega 2023, 8, 28376−28386

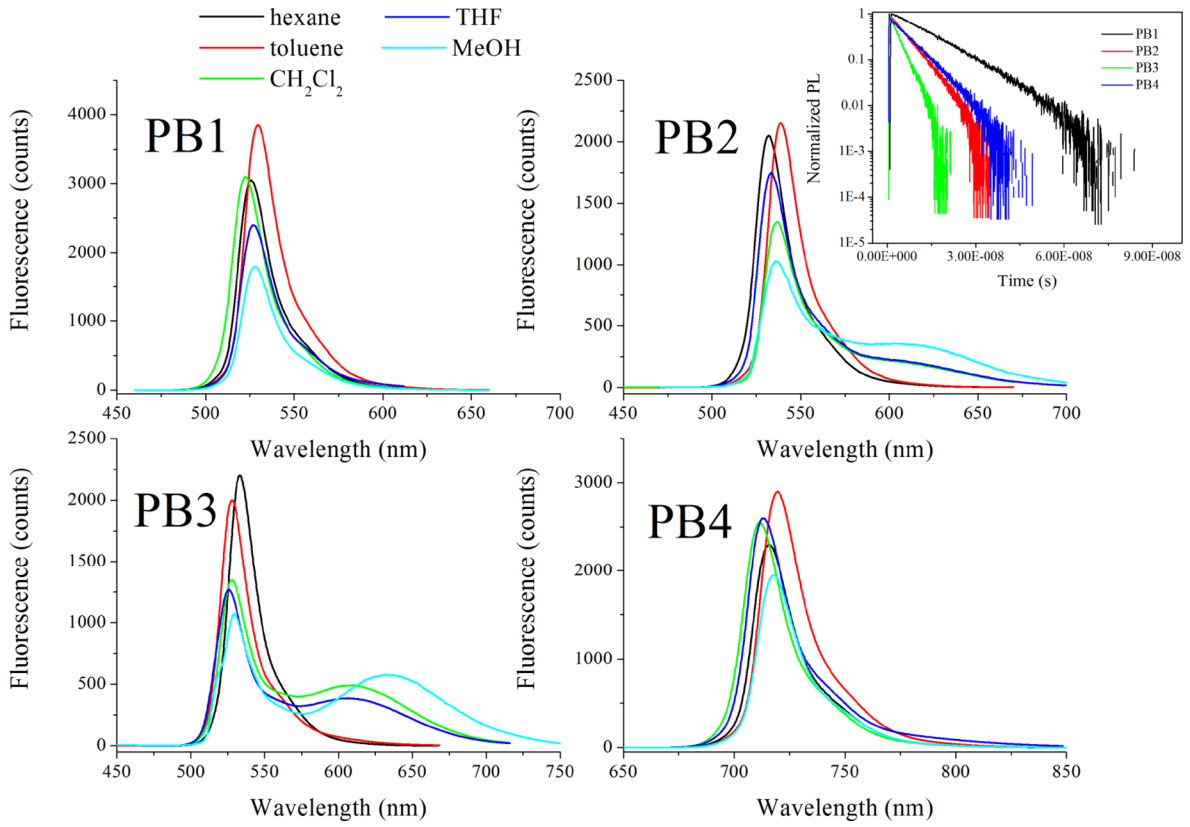

Figure 4. Emission spectra of PB1−PB4 in various solvents (1 μM, λ_{ex} = 500 nm for PB1−PB3, and 680 nm for PB4). Inset: Emission decay dynamics of PB1−PB4, recorded in toluene (1 μM), fitted by $y = y_0 + c \times e^{(-x/t)}$; see the Supporting Information for detailed fitting equations and coefficients.

the purpose of introducing methyl and ethyl groups into these BODIPY dyes was to improve their solubility. The absorption spectra of PB1−PB4 in several representative solvents, including hexane, toluene, CH_2Cl_2, THF, and MeOH, are shown in Figure 3. Good solubility in these solvents was observed. As for PB1−PB3, their absorption spectra are composed of a major absorption band peaking at ∼510 nm and several absorption bands in the UV region (250−400 nm). The first absorption band (∼510 nm) is assigned as the $\pi-\pi^*$ transition of the BODIPY skeleton, and the following ones (250−400 nm) can be attributed to p$-\pi^*$ transitions from N to the pyrrole ring.[18,19] There are only slight spectral shifts between PB1, PB2, and PB3 with their increasing molecular size, as shown in Table 2. This result suggests that the conjugation is ineffective in PB2 and PB3, owing to their twisted confirmation. As for PB4, its $\pi-\pi^*$ transition absorption is red shifted to ∼698 nm, which falls in the bio-active optical window (650−900 nm). It is clear that the fused coplanar conjugation plane is effective in decreasing the energy gap/transition energy between HOMO and LUMO. This observation is consistent with the statement in Section 3.2.

The emission spectra of PB1−PB4 in several representative solvents, including hexane, toluene, CH_2Cl_2, THF, and MeOH, are shown in Figure 4. As for PB1, typical BODIPY emission peaking at 523−530 nm is observed, with an emission quantum yield (Φ) ranging from 0.36 to 0.77. It is observed that the solvent dipole affects both the emission wavelength and emission quantum yield. Generally, a polar solvent leads to an emission red shift and decreased Φ, owing to the strong interaction between the BODIPY excited state and the solvent molecule. A similar case is observed for the other three BODIPY dyes. Additionally, PB2 and PB3 have two emission bands in polar solvents, a major one peaking at ∼530 nm and a shoulder one peaking at ∼615 nm. The former one comes from the BODIPY skeleton, and the latter one shall be attributed to the exciplex or dimer in the excited state.[20] The presence of the shoulder emission band actually suggests a configuration variation/energy competing in the excited state, leading to the decreased emission quantum yield of PB2 and PB3, compared to that of PB1. As for PB4, its fused and coplanar structure successfully decreases the energy gap between HOMO and LUMO, as mentioned above, and thus leads to a NIR emission peaking at ∼720 nm, which falls in the bio-active optical window, with an acceptable emission quantum yield ranging from 0.39 (in MeOH) to 0.58 (in toluene).

After a full comparison of the photophysical parameters in various solvents listed in Table 2, it appears that a high solvent polarity tends to compromise the photophysical performance since solvent molecules may interact with dyes in the excited state, showing a decreased fluorescence quantum yield. Toluene is a proper solvent for PB1−PB4, with a relatively high emission quantum. Then, the lifetime values of PB1−PB4 are determined in toluene for comparison. It is observed from Figure 4 inset that PB1−PB4 emission follows a single exponential decay mode. PB1 shows the longest lifetime among these four dyes as 13.1 ns. As for PB2 and PB3, due to the energy competing from their shoulder emission band (exciplex or dimer in the excited state), their lifetime values are decreased to 5.7 and 2.9 ns, respectively. As for PB4, its

https://doi.org/10.1021/acsomega.3c02452
ACS Omega 2023, 8, 28376−28386

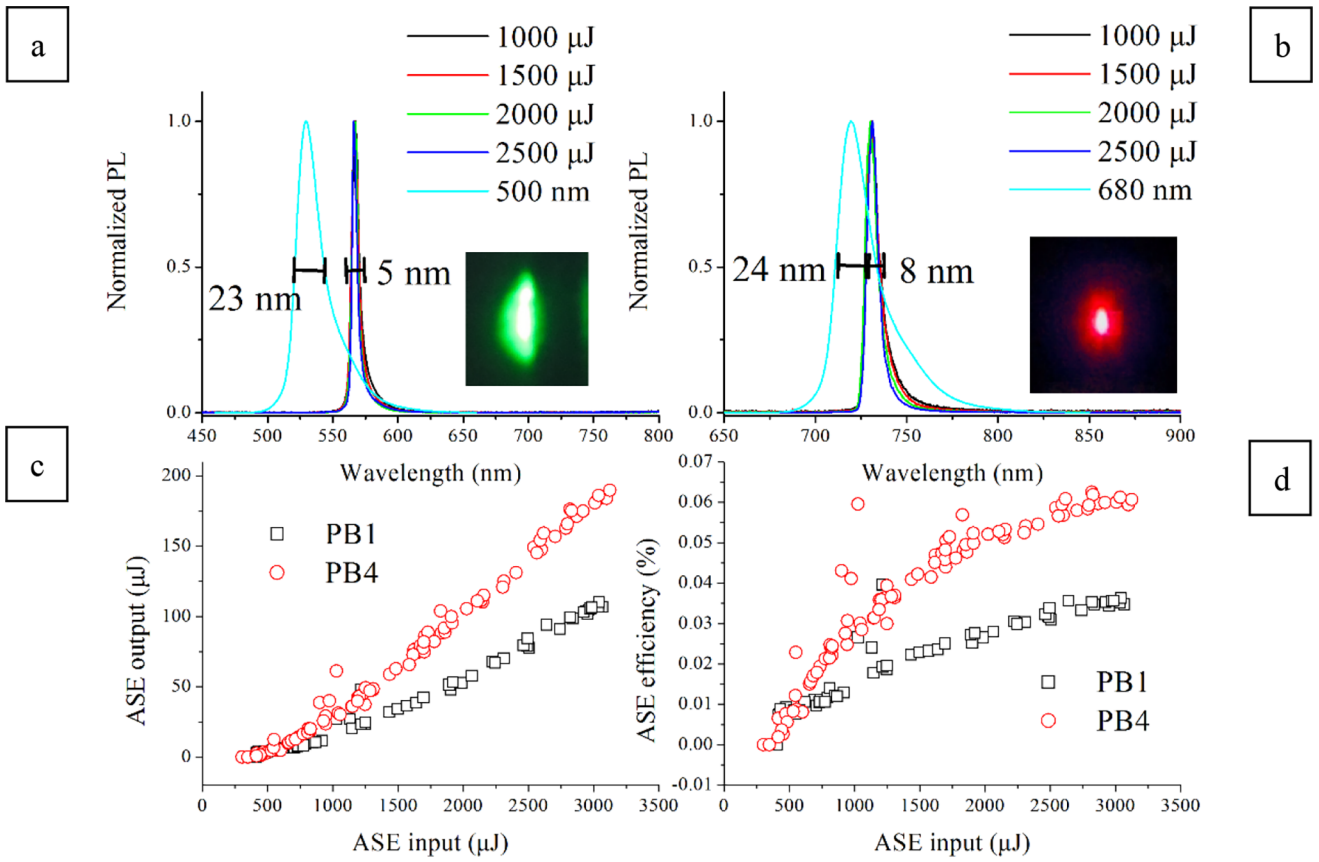

Figure 5. Emission and ASE spectra of PB1 (a) and PB4 (b) upon Xe lamp and 980 nm laser excitation. ASE output (c) and efficiency (d) against increasing pumping energy of PB1 and PB4. Inset photos: ASE beams of PB1 (inset a) and PB4 (inset b) upon 980 nm laser excitation.

lifetime is determined as 7.1 ns. A long excited state lifetime shall be helpful for further applications, such as organic lasing, bio-imaging, and PDT.

3.4. Organic Lasing: ASE Effect. Considering the large fused coplanar plane (confirmed in Section 3.1), the high oscillator strength and polarization ratio of PB4 (confirmed in Section 3.2), and the high emission quantum yield (confirmed in Section 3.3), the ASE performance of PB4, along with that of PB1−PB3, is explored. The ASE effect is observed for PB1 and PB4 with threshold energy values of 1031 and 812 μJ, respectively, as listed in Table 2. But no ASE effect is observed for PB2 and PB3, which is attributed to their low Φ values and their shoulder emission bands, which come from the exciplex or dimer in the excited state.[20] The structural relaxation and vibration of such an exciplex or dimer exhaust an excited state energy, resulting in the absence of the ASE effect.

The photoluminescence spectra of PB1 and PB4 upon a Xe lamp and Nd:YAG laser are compared and shown in Figure 5. Upon Xe lamp excitation, the FWHM (full width at half-maximum) of PB1 is 23 nm, while upon Nd:YAG laser excitation, its FWHM value is decreased to 5 ± 1 nm. In addition, the PB1 ASE peak is red shifted to 566 nm, compared to the PB1 normal emission peaking at 530 nm. As for PB4, its FWHM value upon Nd:YAG laser excitation is decreased to 8 nm, compared to that upon Xe lamp excitation (24 nm). A red shift is still observed for the ASE band peaking at 730 nm. This observation is consistent with the definition of ASE. The corresponding ASE output efficiency is calculated by the ratio of output power against the input one. It is observed from Figure 5 that the ASE efficiency of PB1 is ∼3.5% at a pumping energy of 3000 μJ, while that of PB4 is 6.0% at the same pumping energy. This increased ASE efficiency is explained by the fused coplanar plane of PB4 having a strong oscillator strength, high polarization ratio, and restricted structural relaxation in the excited state. Nevertheless, these ASE efficiency values are still yet to be satisfied. It is assumed that the vibration, relaxation, and distortion of alkyl groups should be responsible for the energy loss in the excited state. Some literatures have mentioned a possible way to substitute −C−H with −C−F, so that the energy loss caused by the vibration, relaxation, and distortion of alkyl groups can be decreased.[21]

3.5. Bio-Application: In Vitro/In Vivo PDT Performance and Bio-Imaging. The PDT application of PB1−PB4 is first discussed by their in vitro $^1O_2$ generation experiment, which uses DPBF as a trapper.[22−27] DPBF inversely reacts with $^1O_2$ and decreases its characteristic absorbance at ∼415 nm. For comparison, PB1−PB4 are exposed to Xe lamp excitation and Nd:YAG laser excitation, and the corresponding absorbance variation is monitored against increasing radiation time, as shown in Figure 6. In the absence of the photosensitizer, DPBF absorbance at 415 nm is rather stable. Upon Xe lamp radiation, DPBF absorbance at 415 nm is gradually decreased by all four BODIPY dyes. PB4 shows the best photodynamic performance due to its fused coplanar plane, high emission quantum yield, and long lifetime. Upon 980 nm radiation, however, DPBF absorbance at 415 nm is only decreased by PB4, while the other three BODIPY dyes fail to do so. This observation is consistent with the above theoretical calculation result, which states that the $TPA_{1,2}$

https://doi.org/10.1021/acsomega.3c02452
ACS Omega 2023, 8, 28376−28386

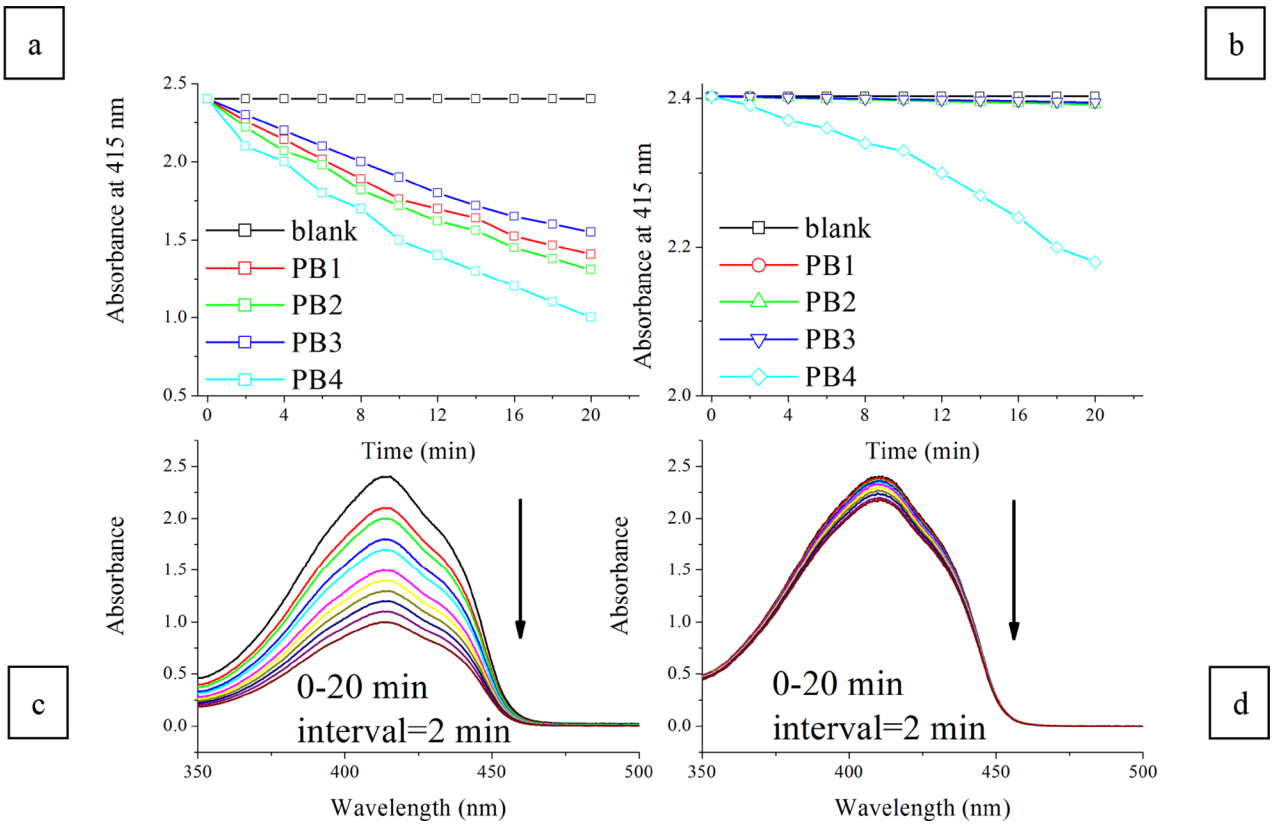

Figure 6. Absorbance variation at 415 nm of DPBF solution (1 mM, in ethanol) with various photosensitizers (0.5 mM) upon Xe lamp radiation (a, 500 nm for PB1−PB3 and 680 nm for PB4) and 980 nm laser radiation (b). Absorption spectra of DPBF (1 mM, in ethanol) with PB4 (0.5 mM) upon Xe lamp radiation (c, 680 nm) and 980 nm laser radiation (d).

oscillator strength of PB4 (0.6771) is nearly 100-fold higher than that of PB1 (0.0098). It should be mentioned that, generally speaking, a fluorescent dye with high fluorescence quantum yield should be inefficient in transferring energy to O_2 and thus in generating $^1O_2$. But PB4 shows an improved PDT performance with an acceptable fluorescence quantum yield, as shown in Table 2. There is a possible mechanism called "singlet fission" to generate a triplet state, as described below by Formula 2. Briefly speaking, one PB4 molecule in the singlet excited state interacts with another PB4 molecule in the ground state to give two PB4 molecules in the triplet state. Then, the PB4 molecules in the triplet state interact with $^3O_2$ to give $^1O_2$. Such a "singlet fission" mechanism has been reported and confirmed by literatures.[28,29] PB4 may follow this "singlet fission" mechanism to satisfy both the high PDT efficiency and high fluorescence quantum yield.

$$^1PB4^* + PB4 \rightleftharpoons {}^3PB4^* + {}^3PB4^* \quad (2)$$

where * means the excited state.

For a further confirmation on the potential bio-application of PB4, a cell endocytosis experiment is performed by a bio-imaging method, as shown in Figure 7. Upon being incubated for 1 h, deep-red emission can be observed. By increasing the incubation time to 5 h, the red emission becomes brighter. This observation suggests that the cell endocytosis for PB4 is time dependent. In other words, PB4 can be effectively absorbed by a progress of cell endocytosis. Then, in vivo $^1O_2$ generation is confirmed by the DCFH-DA/PB4 co-stain experiment. Here, DCFH-DA serves as a fluorescent probe for $^1O_2$ by emitting bright green emission in the presence of

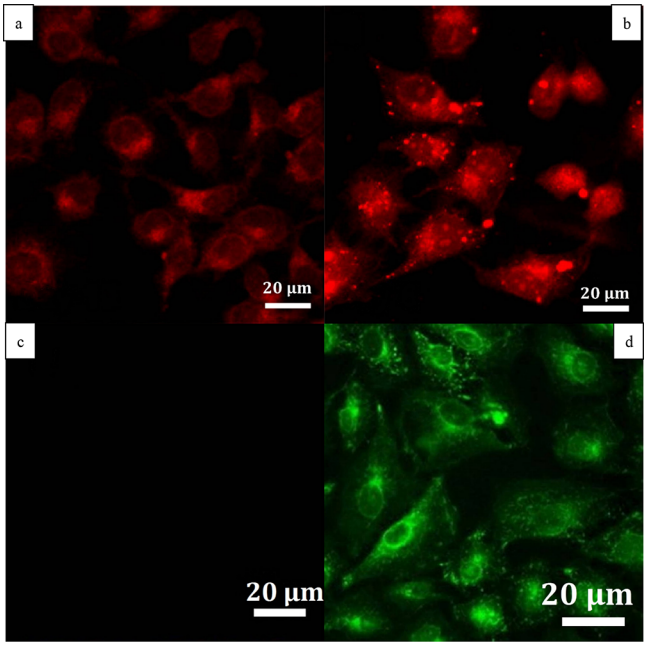

Figure 7. HeLa cells incubated with PB4 for 1 h (a) or 5 h (b); HeLa cells incubated with DCFH-DA/PB4 upon the dark (c) or 980 nm laser (d, 0.6 W/cm^2).

$^1O_2$. As shown in Figure 7, in the absence of 980 nm laser radiation, no green emission is observed. Upon 980 nm radiation, bright green emission is observed, indicating the

https://doi.org/10.1021/acsomega.3c02452
ACS Omega 2023, 8, 28376−28386

release of $^1O_2$ from PB4. As a result, the in vivo $^1O_2$ generation of PB4 is confirmed.

Finally, the PDT efficiency of PB4 is evaluated by cell availability using the MTT method.[30−34] It is observed from Figure 8 that a high cell viability of 91.2% is observed at a PB4

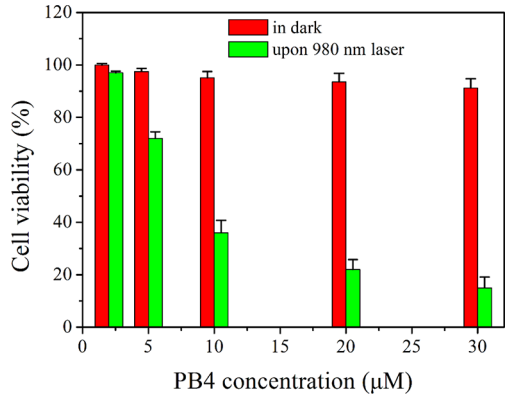

Figure 8. Cell viability of PB4 in various concentrations upon the 980 nm laser or dark.

concentration of 30 μM after being incubated for 24 h, which means that PB4 has low cell cytotoxicity. Upon a 980 nm laser radiation of 5 min, the cell viability is obviously decreased to ∼15%. This result confirms the PDT effect of PB4. As a conclusion, PB4 shows a promising ASE and PDT performance owing to its fused coplanar bisBODIPY structure, which yields deep-red absorption/emission with a high emission quantum yield.

4. CONCLUSIONS

To sum up, four BODIPY dyes were synthesized and confirmed by NMR, MS, elemental analysis, and single-crystal analysis. Their electronic structure, along with OPA and TPA, was revealed by the TD-DFT method. Their absorption/emission spectra, emission quantum yields, and lifetimes were compared. It was found that the fused coplanar structure successfully red shifted PB4 absorption/emission to the deep-red region (698/720 nm), with a quantum yield of 0.58. PB4 showed the ASE effect with an output efficiency of 6.0% at a pumping power of 3000 μJ. An improved PDT performance was observed from PB4 via the in vitro and in vivo experiment. The practical PDT performance was evaluated by cell availability. Upon a 980 nm laser radiation of 5 min, the cell viability was decreased to ∼15%. After a full comparison between PB1 and PB4, it was found that PB4 showed a promising ASE and PDT performance owing to its fused coplanar bisBODIPY structure, which shifted PB4 absorption/emission to the deep-red region with a high emission quantum yield. The methyl and ethyl groups indeed improved the BODIPY solubility but compromised the emission quantum yield by structural relaxation in the excited state. For further efforts, the emission quantum yield should be improved.

■ ASSOCIATED CONTENT

Supporting Information

The Supporting Information is available free of charge at https://pubs.acs.org/doi/10.1021/acsomega.3c02452.

Detailed geometric parameters of PB1−PB4; TD-DFT calculation (by GAMESS 2021) result of PB1−PB4; NMR spectra of PB1−PB4; emission decay fitting equations and coefficients of PB1−PB4 (PDF)

■ AUTHOR INFORMATION

Corresponding Author

Yang Wang − *School of Physical Science and Technology, Southwest Jiaotong University, Chengdu 611756, China;* orcid.org/0000-0001-8205-005X; Email: yangwang@swjtu.edu.cn

Authors

Qinning Sun − *School of Physical Science and Technology, Southwest Jiaotong University, Chengdu 611756, China*

Lei Xie − *School of Physical Science and Technology, Southwest Jiaotong University, Chengdu 611756, China*

Long Chen − *School of Physical Science and Technology, Southwest Jiaotong University, Chengdu 611756, China*

Fengrong Zhu − *School of Physical Science and Technology, Southwest Jiaotong University, Chengdu 611756, China*

Liang Liu − *School of Materials Science & Engineering, Jiangsu University, Zhenjiang 212013, P. R. China;* orcid.org/0009-0002-6278-7315

Complete contact information is available at: https://pubs.acs.org/10.1021/acsomega.3c02452

Notes

The authors declare no competing financial interest.

■ ACKNOWLEDGMENTS

This work is supported by the funding from the National Development and Reform Commission in China (grant numbers Q110522S07001 and Q110523S07001). It is also supported by the Fundamental Research Funds for the Central Universities (grant number 2682020CX77).

■ REFERENCES

(1) Tan, W.; Kopelman, R. Nanoscopic optical sensors and probes. In *Handbook of Nanostructured Materials and Nanotechnology*, Nalwa, H.S., Ed., Academic Press: New York, 2000; pp. 621−667, DOI: 10.1016/B978-012513760-7/50052-6.

(2) Ruan, S. B.; Chan, C. Y.; Ye, H.; Inada, K.; Bencheikh, F.; Sandanayaka, A. S. D.; Matsushima, T.; Adachi, C. A spirofluorene-end-capped bis-stilbene derivative with a low amplified spontaneous emission threshold and balanced hole and electron mobilities. *Opt. Mater.* **2020**, *100*, 109636.

(3) Hanczyc, P.; Słota, P.; Radzewicz, C.; Fita, P. Two-photon excited lasing for detection of amyloids in brain tissue. *J. Photochem. Photobiol., B* **2022**, *228*, 112392.

(4) Yuan, L.; Lin, W.; Zheng, K.; He, L.; Huang, W. Far-red to near infrared analyte-responsive fluorescent probes based on organic fluorophore platforms for fluorescence imaging. *Chem. Soc. Rev.* **2013**, *42*, 622−661.

(5) Loudet, A.; Burgess, K. BODIPY Dyes and Their Derivatives: Syntheses and Spectroscopic Properties. *Chem. Rev.* **2007**, *107*, 4891−4932.

(6) Su, D.; Oh, J.; Lee, S.-C.; Lin, J. M.; Sahu, S.; Yu, X.; Kim, D.; Chang, Y.-T. Dark to light! A new strategy for large Stokes shift dyes: coupling of a dark donor with tunable high quantum yield acceptors. *Chem. Sci.* **2014**, *5*, 4812−4818.

(7) Yu, C.; Jiao, L.; Li, T.; Wu, Q.; Miao, W.; Wang, J.; Wei, Y.; Mu, X.; Hao, E. Fusion and planarization of bisBODIPY: a new family of photostable near infrared dyes. *Chem. Commun.* **2015**, *51*, 16852−16855.

(8) Felion, C.; Lopez-Gonzalez, R.; Sewell, A. L.; Marquez, R.; Gauchotte-Lindsay, C. BODIPY-labeled estrogens for fluorescence

analysis of environmental microbial degradation. *ACS Omega* **2022**, *7*, 41284−41295.
(9) Wang, D.; Wang, X.; Zhou, S.; Gu, P.; Zhu, X.; Wang, C.; Zhang, Q. Evolution of BODIPY as triplet photosensitizers from homogeneous to heterogeneous: The strategies of functionalization to various forms and their recent applications. *Coord. Chem. Rev.* **2023**, *482*, 215074.
(10) Cheng, H.-B.; Cao, X.; Zhang, S.; Zhang, K.; Cheng, Y.; Wang, J.; Zhao, J.; Zhou, L.; Liang, X.-J.; Yoon, J. BODIPY as a multifunctional theranostic reagent in biomedicine: self-assembly, properties, and applications. *Adv. Mater.* **2023**, *35*, 2207546.
(11) Nguyen, V.-N.; Yim, Y.; Kim, S.; Ryu, B.; Swamy, K. M. K.; Kim, G.; Kwon, N.; Kim, C.-Y.; Park, S.; Yoon, J. Molecular design of highly efficient heavy-atom-free triplet bodipy derivatives for photodynamic therapy and bioimaging. *Angew. Chem., Int. Ed.* **2020**, *59*, 8957−8962.
(12) Gündüz, E. Z.; Tasasiz, B.; Gedik, M. E.; Günaydin, G.; Okutan, E. NI-BODIPY-GO Nanocomposites for Targeted PDT. *ACS Omega* **2023**, *8*, 8320−8331.
(13) Kolemen, S.; Işik, M.; Kim, G. M.; Kim, D.; Geng, H.; Buyuktemiz, M.; Karatas, T.; Zhang, X.-F.; Dede, Y.; Yoon, J.; Akkaya, E. U. Intracellular modulation of excited-state dynamics in a chromophore dyad: Differential enhancement of photocytotoxicity targeting cancer cells. *Angew. Chem., Int. Ed.* **2015**, *54*, 5340−5344.
(14) Bennniston, A. C.; Copley, G.; Elliott, K. J.; Harrington, R. W.; Clegg, W. Redox-Controlled Fluorescence Modulation in a BODIPY-Quinone Dyad. *Eur. J. Org. Chem.* **2008**, *2008*, 2705−2713.
(15) Li, R.; Mulder, T. A.; Beckmann, U.; Boyd, P. D. W.; Brooker, S. Dicopper(II) and dinickel(II) complexes of Schiff-base macrocycles derived from 5,5-dimethyl-1,9-diformyldipyrromethane. *Inorg. Chim. Acta* **2004**, *357*, 3360−3368.
(16) Zhang, L.; Li, B. A series of Eu(III) emitters with a novel triphenylamine-derived beta-diketone ligand. *J. Lumin.* **2009**, *129*, 1304−1308.
(17) Zhang, L.; Li, B. A series of 4,5-diazafluoren-9-one-derived ligands and their Cu(I) complexes: Synthesis, characterization and photophysical properties. *Inorg. Chim. Acta* **2009**, *362*, 4857−4861.
(18) Bruhn, T.; Pescitelli, G.; Jurinovich, S.; Schaumlöffel, A.; Witterauf, F.; Ahrens, J.; Bröring, M.; Bringmann, G. Axially Chiral BODIPY DYEmers: An Apparent Exception to the Exciton Chirality Rule. *Angew. Chem., Int. Ed.* **2014**, *53*, 14592−14595.
(19) Grzybowski, M.; Skonieczny, K.; Butenschön, H.; Gryko, D. T. Comparison of Oxidative Aromatic Coupling and the Scholl Reaction. *Angew. Chem., Int. Ed.* **2013**, *52*, 9900−9930.
(20) Nepomnyashchii, A. B.; Bröring, M.; Ahrens, J.; Brad, A. J. Chemical and Electrochemical Dimerization of BODIPY Compounds: Electrogenerated Chemiluminescent Detection of Dimer Formation. *J. Am. Chem. Soc.* **2011**, *133*, 19498−19504.
(21) Li, H.; Liu, X.; Lyu, C.; Ma, F.; Ye, H.; Wyatt, P. B.; Gillin, W. P. Enhanced 1.54 lm luminescence of a perfluorinated erbium complex sensitized by perfluorinated Pt(II) and Zn(II) phthalocyanines with 980 nm emission. *J. Mater. Chem. C* **2020**, *9*, 456−465.
(22) Zhang, W.; Li, B.; Ma, H.; Zhang, L.; Guan, Y.; Zhang, Y.; Zhang, X.; Jing, P.; Yue, S. Combining Ruthenium(II) Complexes with Metal−Organic Frameworks to Realize Effective Two-Photon Absorption for Singlet Oxygen Generation. *ACS Appl. Mater. Interfaces* **2016**, *8*, 21465.
(23) Ding, Y.; Tang, Y.; Zhu, W.; Xie, Y. Fluorescent and colorimetric ion probes based on conjugated oligopyrroles. *Chem. Soc. Rev.* **2015**, *44*, 1101−1112.
(24) Ulrich, G.; Ziessel, R.; Harriman, A. The Chemistry of Fluorescent Bodipy Dyes: Versatility Unsurpassed. *Angew. Chem., Int. Ed.* **2008**, *47*, 1184−1201.
(25) Benniston, A. C.; Copley, G. Lighting the way ahead with boron dipyrromethene (Bodipy) dyes. *Phys. Chem. Chem. Phys.* **2009**, *11*, 4124−4131.
(26) Ni, Y.; Wu, J. Far-red and near infrared BODIPY dyes: synthesis and applications for fluorescent pH probes and bio-imaging. *Org. Biomol. Chem.* **2014**, *12*, 3774−3791.
(27) Wang, F.; Zhou, L.; Zhao, C.; Wang, R.; Fei, Q.; Luo, S.; Guo, Z.; Tian, H.; Zhu, W. −. H. A dual-response BODIPY-based fluorescent probe for the discrimination of glutathione from cystein and homocystein. *Chem. Sci.* **2015**, *6*, 2584−2589.
(28) Wang, L.; Lin, L.; Yang, J.; Wu, Y.; Wang, H.; Zhu, J.; Yao, J.; Fu, H. Singlet Fission in a Pyrrole-Fused Cross-Conjugated Skeleton with Adaptive Aromaticity. *J. Am. Chem. Soc.* **2020**, *142*, 10235−10239.
(29) Wu, Y.; Wang, Y.; Chen, J.; Zhang, G.; Yao, J.; Zhang, D.; Fu, H. Intramolecular Singlet Fission in an Antiaromatic Polycyclic Hydrocarbon. *Angew. Chem., Int. Ed.* **2017**, *56*, 9400−9404.
(30) Wang, S.; Du, Y.; Zhang, J.; Chen, G. Rod-like BODIPY nanomaterials with enhanced photodynamic activity. *New J. Chem.* **2020**, *44*, 11324−11329.
(31) Jiao, L.; Yu, C.; Uppal, T.; Liu, M.; Li, Y.; Zhou, Y.; Hao, E.; Hu, X.; Vicente, M. G. H. Long wavelength red fluorescent dyes from 3,5-diiodo-BODIPYs. *Org. Biomol. Chem.* **2010**, *8*, 2517−2519.
(32) Zhao, N.; Xuan, S.; Fronczek, F. R.; Smith, K. M.; Vicente, M. G. H. Stepwise Polychlorination of 8-Chloro-BODIPY and Regioselective Functionalization of 2,3,5,6,8-Pentachloro-BODIPY. *J. Org. Chem.* **2015**, *80*, 8377−8383.
(33) Zhao, N.; Vicente, M. G. H.; Fronczek, F. R.; Smith, K. M. Synthesis of 3,8-Dichloro-6-ethyl-1,2,5,7-tetramethyl−BODIPY from an Asymmetric Dipyrroketone and Reactivity Studies at the 3,5,8-Positions. *Chem. − Eur. J.* **2015**, *21*, 6181−6192.
(34) Bergström, F.; Mikhalyov, I.; Hägglöf, P.; Wortmann, R.; Ny, T.; Johansson, L. B.-Å. Dimers of Dipyrromethene boron Difluoride (BODIPY) with Light Spectroscopic Applications in Chemistry and Biology. *J. Am. Chem. Soc.* **2002**, *124*, 196−204.

https://doi.org/10.1021/acsomega.3c02452
ACS Omega 2023, 8, 28376−28386